Journal of Applied Polymer Science

In situ fibrillation of polypropylene/polyamide 6 blends: Effect of organoclay addition

Dimitri Chomat,[1] Jérémie Soulestin,[1] Marie-France Lacrampe,[1] Michel Sclavons,[2] Patricia Krawczak[1]

[1]Mines Douai, Department of Polymers and Composites Technology and Mechanical Engineering, 941 rue Charles Bourseul, CS 10838, F-59508 Douai, France

[2]Bio- and Soft Matter, Institute of Condensed Matter and Nanosciences, Université Catholique de Louvain, Louvain-la-Neuve, Belgium

Correspondence to: J. Soulestin (E-mail: jeremie.soulestin@mines-douai.fr)

ABSTRACT: *In situ* fibrillation of PP/PA6 blends (85/15 wt %) is investigated in presence of two kinds of organically modified montmorillonite, differing by the polarity of their surfactant. The organoclay is primary dispersed either in the PP (for the low-polarity Cloisite® 15A) or in the PA6 (for the high-polarity Cloisite® 30B), according to its assumed affinity. In absence of organoclay, a fibrillar morphology is achieved after the melt-blending and hot-stretching step, as evidenced by SEM analysis. Upon clay addition, different morphological trends are evidenced. The C15A leads to a refinement of the fibrils whether the C30B induces a transition from fibrillar to nodular structure. These trends are ascribed to drastic changes in viscosity and elasticity ratios, due to the filler initial localization. Several techniques (DSC, STEM) point out a C15A migration from the PP to the PP/PA6 interface. Rheological measurements highlight the possibility of a double-percolation phenomenon, linked to the fibrillar microstructure of the PP/PA6/C15A blend.
 J. Appl. Polym. Sci. **2015**, *132*, 41680.

KEYWORDS: blends; composites; polyamides; polyolefins; viscosity and viscoelasticity

Received 18 July 2014; accepted 23 October 2014
DOI: 10.1002/app.41680

INTRODUCTION

Polypropylene (PP) and polyamide 6 (PA6) are the most used polymers in the automotive industry. Although these two materials are known to be incompatible—i.e. they present a high interfacial tension—new recycling directives will involve an important gain of interest in PP/PA6 blends in years to come. The development of a polymer/polymer composite with fibrillar morphology, based on this couple of polymers, could thus be a challenging task since this kind of structure enhances the matrix mechanical performances while keeping the processing flexibility of a thermoplastic.

Such composites may be developed using a three-step *in situ* fibrillation process.[1] First, a melt blending is performed so as to disperse finely the minor phase in the matrix. During this step, the morphology is controlled by two main parameters: the capillary number *Ca* (ratio between shear forces and interfacial forces) and the viscosity ratio *k*. The dispersion is effective when the capillary number overcome a critical value, leading to the splitting of a particle into sub-particles. It has been reported a lot of times that, in pure shear flow, for Newtonian systems, a viscosity ratio $k > 4$ restrains this mechanism by turning the critical *Ca* to infinite.[2] The viscosity ratio should thus be kept below that value; else a poor dispersion is attained. In the case of viscoelastic materials, the elasticity ratio *k'* becomes important as well. Actually, studies demonstrated that matrix elasticity helps the deformation process, whereas minor phase elasticity inhibits deformation.[3,4] To promote the dispersion and thereafter the fibrillation, it is thus necessary to develop a system such as $k < 4$ and $k' < 1$.

After the melt blending, the microstructure is supposed to be nodular. A second step, namely the fibrillation step, consists in stretching the extruded strand in a drawing device.[5] Consequently, the extensional forces help turning the spherical particles into well oriented short fibrils. Simultaneously, the strand diameter constriction favors a coalescence phenomenon between these short fibrils and thus the development of several hundred micrometer long fibrils.[6]

Finally, this semi-finished product is processed at low temperature by injection-molding or compression-molding in order to obtain the desired composite parts. During this last step, the minor phase must be kept safely below its melting temperature; otherwise the molten fibrils would likely go back to a nodular

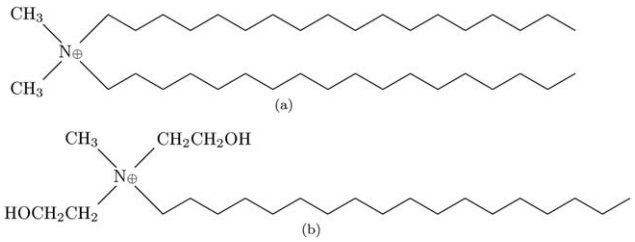

Figure 1. Chemical structure of the surfactant used for Cloisite® C15A modification (a) and for Cloisite® C30B modification (b).

equilibrium shape.[7] The difference between the melting temperature of the major and the minor phase should thus be higher than 30°C in order to have a sufficient processing window.[8]

During the last decade, a lot of studies have dealt with the effect of organoclay addition in immiscible polymer blends. Several authors claim that this kind of nanoparticle can promote compatibilization through different mechanisms. Actually, intercalated or exfoliated organoclay can lead to a reduction of domain size[9,10] and, in some cases, to the transition from two T_gs to only one T_g[11–13] when the particles are located at the interface. This compatibilization may be caused by a reduction of interfacial tension[14] or by the inhibition of the static and dynamic coalescence,[15,16] thanks to a barrier effect.

PP/PA6 blends showing a high interfacial tension, the addition of organoclay could thus be a possible solution in order to improve compatibility. Most of the previous cited studies dealing with nodular morphologies, it is also of particular interest to see how a fibrillar morphology can benefit from the presence of organoclays.

Hence, the present work aims at investigating the effect of organoclay addition on the morphology and the properties of polypropylene/polyamide 6 microfibrillar composites. No additional chemical compatibilization is attempted, in order to avoid any morphological evolution due to interfacial tension reduction or chemical coupling induced by the compatibilizer.

EXPERIMENTAL

Materials

The polymers used for the study are an homopolymer PP (B10FB, Polychim, France) having a melt flow index of 12 g/10 min and an extrusion grade PA6 (Akulon® F136-C1, DSM, The Netherlands). Before processing, the PA6 is dried overnight in a vacuum oven at 80°C. Two kinds of organically modified montmorillonite are used—Cloisite® 15A (C15A) and 30B (C30B) (Southern Clay Products, USA)—differing by the polarity of their cationic surfactants (low polarity for C15A and high polarity for C30B) [Figure 1(a,b)], the montmorillonite itself being highly polar in both cases. The C15A and the C30B contain respectively 43 and 30 wt % of surfactants.

Compounding

Two nanocomposite masterbatches were compounded by twin-screw extrusion (BC45, Clextral, France), according to the affinities between polymers and surfactants: a PP/C15A masterbatch with a mineral fraction of 8.3 wt % and a PA6/C30B masterbatch with a mineral fraction of 9.4 wt %. For the sake of simplicity, the expression "% C15A" and "% C30B" will be used when talking about montmorillonite content (i.e. mineral fraction of Cloisite®) deriving from Cloisite® 15A or Cloisite® 30B, respectively. The PP-C15A masterbatch was subsequently diluted in PP by single-screw extrusion (Haake Rheocord, Germany) in order to obtain PP nanocomposites containing 0.5, 1.1, and 1.6 wt % of clay. Similarly, PA6-C30B masterbatch was diluted in PA6 until clay contents of 3, 6, and 9 wt % were reached.

Melt-Blending and Hot-Stretching

These PP- and PA6-based nanocomposites, containing different amounts of organoclay, were then mixed with neat PA6 and PP, respectively, at a weight ratio of 85/15 (PP/PA6) at 240°C in a twin-screw extruder equipped with a capillary die (Haake Polylab PTW 16/40, Thermo Scientific, Germany) (Table I). After cooling in a water bath, the extrudate was stretched in a drawing device (10 m min^{-1}) and pelletized (Figure 2). A twin-screw extrusion simulation software (Ludovic®) was used to evaluate the shear rate along the screw profile.

Injection-Molding

Test samples were finally injection-molded (Babyplast 6/10P, Cronoplast, Spain) at low temperature (temperature profile ranging from 190 to 205°C) so as to avoid PA6 melting (T_m[PA6] = 222°C).

X-ray Diffraction

XRD analysis (D8 Advance, Bruker, Germany) was performed for angles θ between 2° and 10° (pitch 0.02°) on injection-molded discs (50 mm diameter, 2-mm thick). The apparatus uses a cobalt source with $\lambda = 1.79$ Å, and a monochromator operating at 40 kV (intensity 40 mA). Clay interlayer spacing (d_{001}) was then determined using Bragg's law [eq. (1)].

$$d = \frac{n\lambda}{2\sin\theta} \quad (1)$$

Rotational Dynamic Rheology

A parallel plate rheometer (Haake Mars III, Thermo Scientific, Germany) was used in small amplitude oscillatory mode. Measurements were carried out at 240°C under inert (N_2) atmosphere. All experiments were conducted within the linear viscoelastic range, in a controlled strain mode. Before each experiment, a resting time of ten minutes was applied for temperature equilibration. Post-processing of frequency sweep

Table I. Composition of PP/PA6 and PP/PA6/Clay Blends

Blends	Composition (wt %)	
PP/PA6	85 (PP)	15 (PA6)
PP/PA6/0.45% C15A	85 (PP-0.5% C15A)	15 (PA6)
PP/PA6/0.9% C15A	85 (PP-1.1% C15A)	15 (PA6)
PP/PA6/1.35% C15A	85 (PP-1.6% C15A)	15 (PA6)
PP/PA6/0.45% C30B	85 (PP)	15 (PA6-3% C30B)
PP/PA6/0.9% C30B	85 (PP)	15 (PA6-6% C30B)
PP/PA6/1.35% C30B	85 (PP)	15 (PA6-9% C30B)

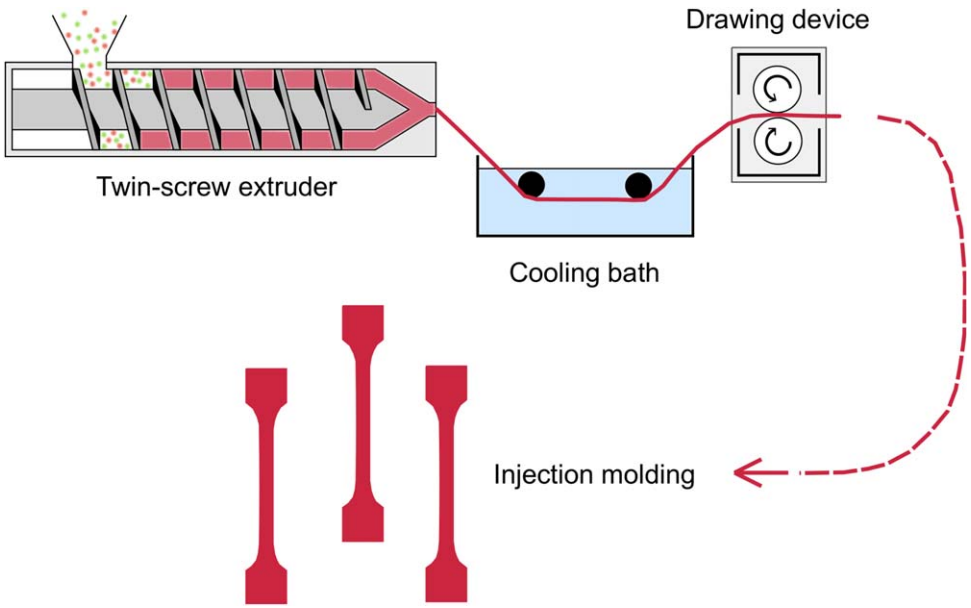

Figure 2. Schematic illustration of the *in situ* fibrillation process. [Color figure can be viewed in the online issue, which is available at wileyonlinelibrary.com.]

rheological data was done with the Spectra tool from Rheowin software. On the basis of a generalized Maxwell model with $\lambda_i = \eta_i/G_i$, this module uses a non-linear Tikhonov regularization to calculate the continuous relaxation spectrum $H(\lambda)$ from the values of G' and G'' [eqs. (2) and (3)].[17]

$$G'(\omega) = \int_0^\infty \frac{H(\omega\lambda)^2}{1+(\omega\lambda)^2} d(\ln\lambda) \quad (2)$$

$$G''(\omega) = \int_0^\infty \frac{H(\omega\lambda)}{1+(\omega\lambda)^2} d(\ln\lambda) \quad (3)$$

Differential Scanning Calorimetry (DSC)

Crystallization temperatures and enthalpies were measured by DSC (DSC 8500, PerkinElmer, USA) under N2 atmosphere, using aluminum ventilated pans. First, the samples were heated to 250°C in order to remove thermal history. The measurements occurred during the subsequent cooling (down to −50°C) and during the second heating (up to 250°C), both at 10°C min^{-1}. Crystallinity was determined considering a theoretical enthalpy value of 209 and 190 J g^{-1} for 100% crystalline PP and PA6, respectively.[18] For accuracy purposes, measurements were conducted twice (a new sample used each time) and then averaged.

Scanning Transmission Electronic Microscopy (STEM)

Clay localization was determined by STEM experiments (Carl Zeiss LEO 922) on thin slices of injected PP/PA6/clay samples, with an accelerated voltage of 30 kV. A Leica Reichert FCS microtome was used for sample preparation.

Scanning Electronic Microscopy (SEM)

Morphology was observed by SEM (S-4300SE/N, Hitachi, Japan) on extruded samples cryofractured along two perpendicular planes so as to get a 3D view of the structure. The samples were gold coated and analyzed at an accelerating voltage of 10 kV. Calculation of an average particle diameter was made by measuring manually a hundred particles, using ImageJ software.

RESULTS AND DISCUSSION

When dealing with polymers filled with nanoclays, one has to ensure of the state of dispersion of the nanofiller. In that purpose, XRD characterization has been performed on the two masterbatches obtained after the first extrusion step (Figure 3). Actually, presence of regularly arranged clay layers results in an X-ray diffraction signal linked to the interlayer spacing, which

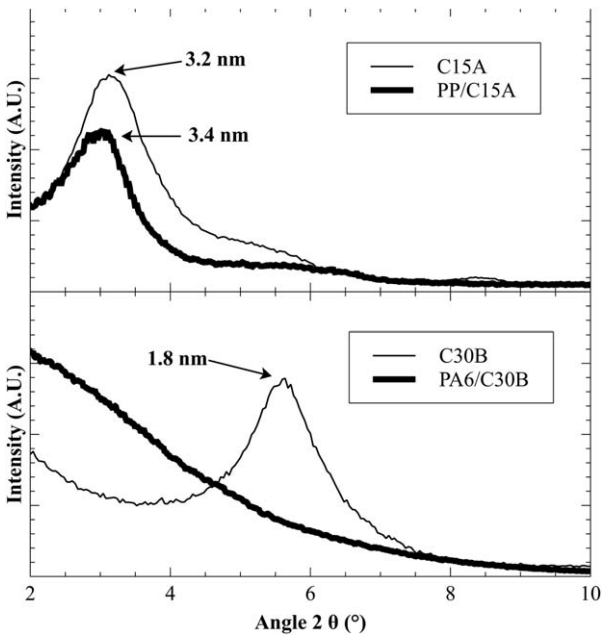

Figure 3. XRD patterns of PP/C15A and PA6/C30B masterbatches.

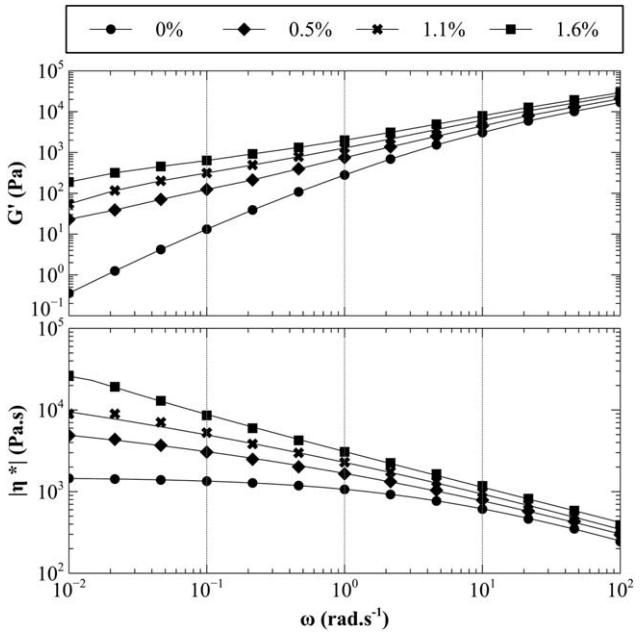

Figure 4. Storage modulus (G') and complex viscosity ($|\eta^*|$) of PP with 0, 0.5, 1.1, and 1.6 wt % of C15A.

enables in particular to evidence the presence of clay tactoids. In the case of PP/C15A, the diffraction peak is only slightly shifted toward the low angles compared to pure C15A, demonstrating that very few macromolecules are able to intercalate inside the clay tactoids. The interlayer spacing hence increases from 3.2 to 3.4 nm. In that masterbatch, the montmorillonite is thus dispersed on a tactoid level as the diffraction peak remains practically unaffected. This is typical of a microcomposite rather than a nanocomposite. For the PA6/C30B masterbatch, the diffraction peak tends to disappear, indicating some exfoliation mechanism, thanks to the affinities between PA6 macromolecules and organo-modified montmorillonite. However, the diffracted intensity increases at low angles, indicating the possible presence of remaining tactoids with various interlayer spacings, in addition to exfoliated platelets. These experiments confirm the already known result that nanoclay dispersion is far easier in a polar polymer (such as PA6) than in an apolar one (such as PP), even with the appropriate surfactants.

To obtain complementary information on nanoclay dispersion, dynamic rheological measurements have been conducted on the diluted nanocomposite compounds. It is important to note that these measurements were done at 240°C, meaning that PA6 is only 15–20°C above its melting temperature whereas PP is 80°C above its T_m. The viscoelastic behavior of these two polymers is thus rather different. As can be seen in Figure 4, the addition of nanoclay induces a clear evolution in the rheological behavior of polypropylene. At low frequency, the storage modulus of PP/C15A microcomposites deviates from the one of pure PP, even for the lowest clay content. The decrease of G' slope in the low-frequency domain (between 0.01 and 0.1 rad s^{-1}) demonstrates that an effective dispersion of the filler is achieved,[19] with a tactoids size reduction. The complex viscosity η^* gives the same information through a huge viscosity increase at low frequency, linked to longer relaxation times. Figure 5 shows a similar trend for PA6/C30B nanocomposites with a more pronounced intensity, thanks to the higher filler contents. At 9% of clay reinforcement, a non-terminal behavior, characteristic of a solid-like material, is achieved, bringing evidence of a percolated network.[20]

To estimate the level of clay dispersion, recent works recommend the use of apparent yield stress (σ_0) rather than G' slope.[21] Actually, the yield stress is a direct indication of physical interactions between particles and grows with the fraction of exfoliated clay platelets. One can thus infer the level of clay dispersion from this value. The apparent yield stress can be determined by fitting the complex viscosity data with a Carreau-Yasuda law including an additional term of yield stress σ_0/ω (ω: angular frequency, η_0: zero-shear viscosity, λ: average relaxation time, n: flow index, a: curvature parameter) [eq. (4)].

$$|\eta^*(\omega)| = \frac{\sigma_0}{\omega} + \eta_0[1+(\lambda\omega)^a]^{(n-1)/a} \quad (4)$$

The results presented in Table II don't show any apparent yield stresses for the PP microcomposites except for the last one, at 1.6% of C15A. Interactions between clay platelets are thus weak, but growing with clay content. Considering the low montmorillonite contents and the known difficulties for dispersing organoclays in a hydrophobic polymer, this result is quite promising. Conversely, PA6 nanocomposites exhibit high yield stresses, up to 45600 Pa for the PA6–9% C30B. This demonstrates without ambiguity the presence of clay percolated networks inside the PA6. Although it may be tempting to ascribe this behavior to fully exfoliated clay platelets, it is important to take into account the high filler content, giving obviously the possibility to form a percolated network without full exfoliation. However, previous studies on PA6 nanocomposites, elaborated using the same procedures, have evidenced the existence of high

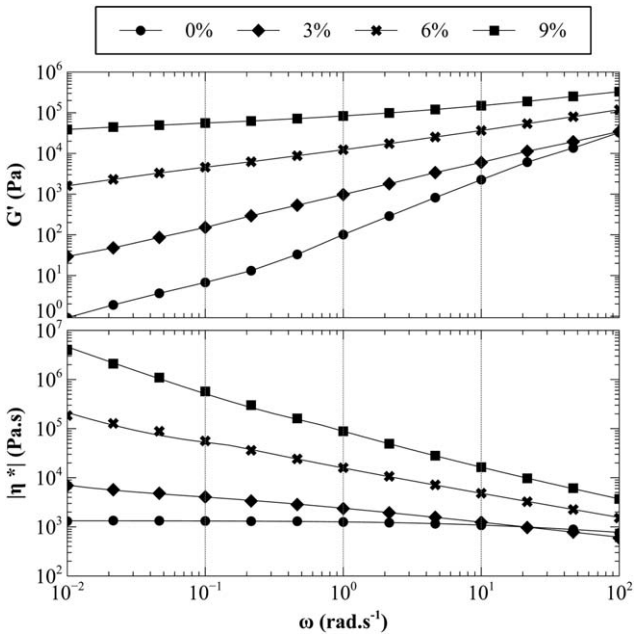

Figure 5. Storage modulus (G') and complex viscosity ($|\eta^*|$) of PA6 with 0, 3, 6, and 9 wt % of C30B.

Table II. Apparent Yield Stress (σ_0) in PP-C15A Microcomposites and PA6-C30B Nanocomposites

Microcomposites	σ_0 (Pa)	Nanocomposites	σ_0 (Pa)
PP	0	PA6	0
PP-0.5% C15A	0	PA6-3% C30B	24
PP-1.1% C15A	0	PA6-6% C30B	1770
PP-1.6% C15A	68	PA6-9% C30B	45600

Values obtained by modified Carreau-Yasuda law regression.

exfoliation rate even at high C30B content.[22,23] This first set of experiments enabled to assess the process efficiency for the development of nanocomposite compounds. Thanks to the good degree of clay dispersion (tactoids of reduced size for PP-C15A, exfoliation for PA6-C30B), optimal conditions are obtained to maximize the effect of the nanofillers on the fibrillation process. The next results will thus be about the blends realized by *in situ* fibrillation, based on PP-C15A and PA6-C30B.

Figure 6 reveals the different morphologies obtained after the drawing process. The transverse view of the neat PP/PA6 blend is characterized by hemispherical shapes and cut-off fibers. Thanks to longitudinal images, a well-defined fibrillar morphology, oriented along the flow direction, can be identified. The *in situ* fibrillation process thus confirms its efficiency. With the addition of C15A, several evolutions are visible. First, the transverse view shows smaller fibrils with more complex shapes. Second, the longitudinal view displays again a lot of oriented fibrils but with shorter lengths and irregular profiles. A specific flaky surface aspect is also ascribed to the addition of C15A. Hence, all these elements demonstrate the importance of clay–polymer interactions and the role of interfacial agent played by the C15A. A very different morphology can be observed with the

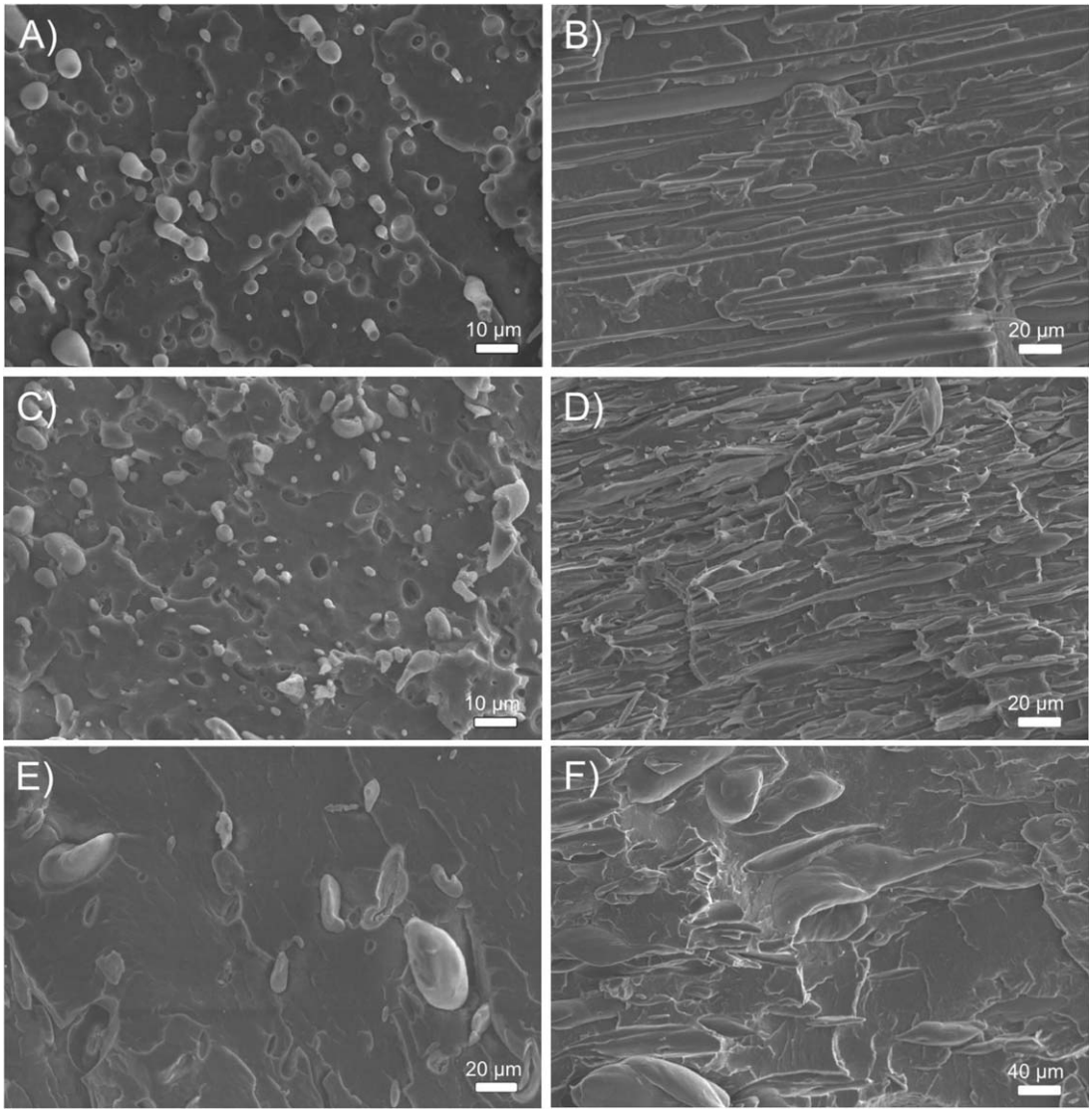

Figure 6. SEM micrographs of cryofractured surfaces of PP/PA6 (A: transversal, B: longitudinal), PP/PA6/1.35% C15A (C: transversal, D: longitudinal) and PP/PA6/1.35% C30B (E: transversal, F: longitudinal).

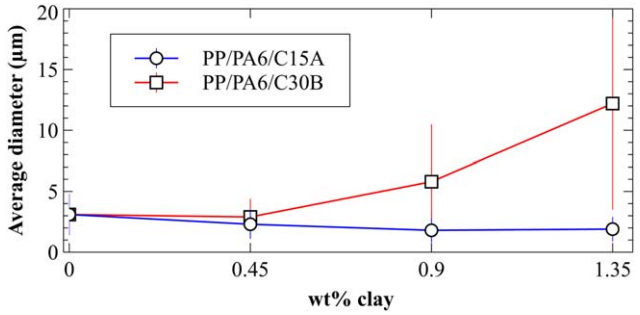

Figure 7. Average diameter of PA6 fibrils in PP/PA6/C15A and PP/PA6/C30B blends, obtained by image analysis of blends cryofractured surfaces. [Color figure can be viewed in the online issue, which is available at wileyonlinelibrary.com.]

PP/PA6/C30B blends. In that latter case, much bigger nodules are visible on the transversal image. The longitudinal view shows that the minor phase is no longer fibrillar as the clay content rises. Instead, one can observe an oriented, roughly nodular morphology, characteristic of a poor dispersion of the minor phase.

For each blend, the average diameter was determined from SEM experiments (Figure 7). The results show a slight fibril thinning upon C15A addition (from 3.1 to 1.9 μm), but have to be tempered as cryofracturing can alter measurement representativity. As expected, the mean diameter increases strongly for PP/PA6/C30B blends (up to 12 μm). Figures 8 and 9 display the distribution of diameters for each blend. It appears clearly that this distribution gets narrower and narrower with C15A addition (Figure 8). In particular, the maximum fibril diameter drops below 5 μm for the highest C15A content, which is consistent with a compatibilizing action. The opposite mechanism happens

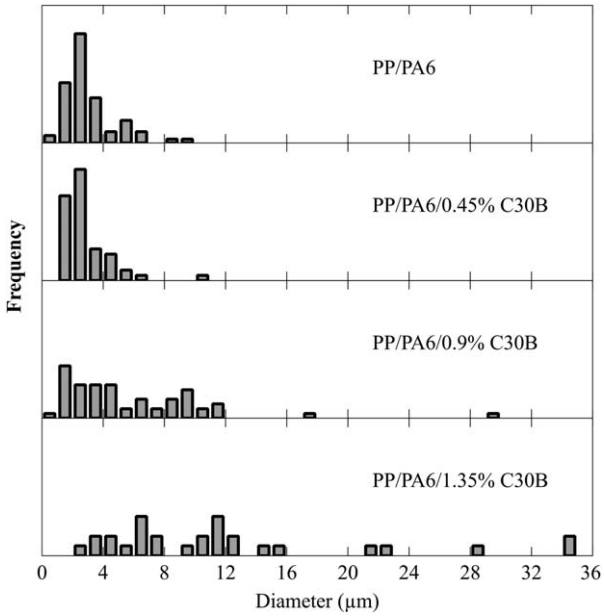

Figure 9. Fibrils diameter distribution of PP/PA6 blends with 0, 0.45, 0.9, and 1.35 wt % of C30B.

with the C30B (Figure 9). The distribution of fibril and nodule diameter widens upon C30B addition, up to a range 0–30 μm.

An explanation for these phenomena can be found considering the viscosity ratios (Figure 10). As reported previously in Figures 4 and 5, adding nanoclay involves a gain in viscosity for the polymer host. So, depending on the clay localization (PP or PA6), the viscosity ratio ($\eta_{(PA6)}/\eta_{(PP)}$) will either increase or decrease. During a twin-screw extrusion process, it has been demonstrated that most of the microstructural changes take place at the very beginning of the extruder.[24,25] Hence, we

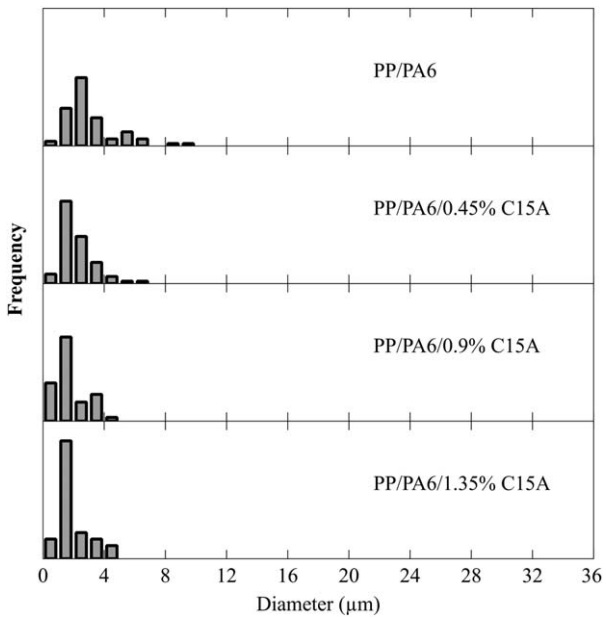

Figure 8. Fibrils diameter distribution of PP/PA6 blends with 0, 0.45, 0.9, and 1.35 wt % of C15A.

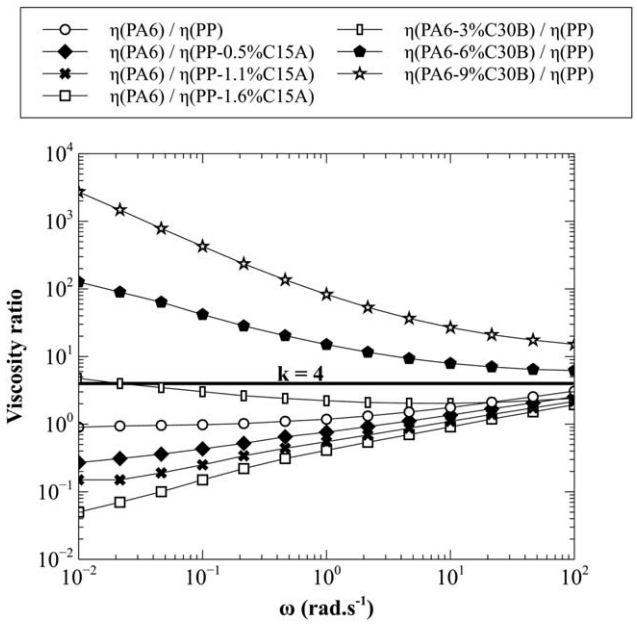

Figure 10. Viscosity ratio of PP/PA6 and PP/PA6/clay blends (the horizontal line highlights a critical viscosity ratio of 4).

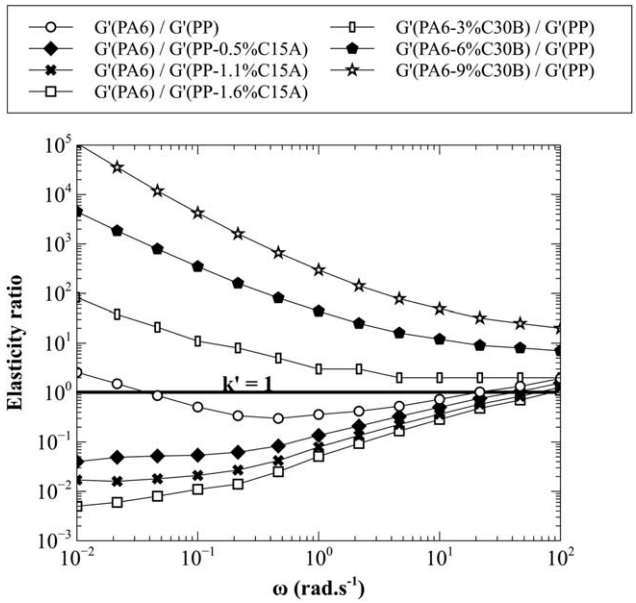

Figure 11. Elasticity ratio of PP/PA6 and PP/PA6/clay blends (the horizontal line highlights an elasticity ratio of 1). The elasticity ratio is defined as *G*'(minor phase)/*G*'(matrix).

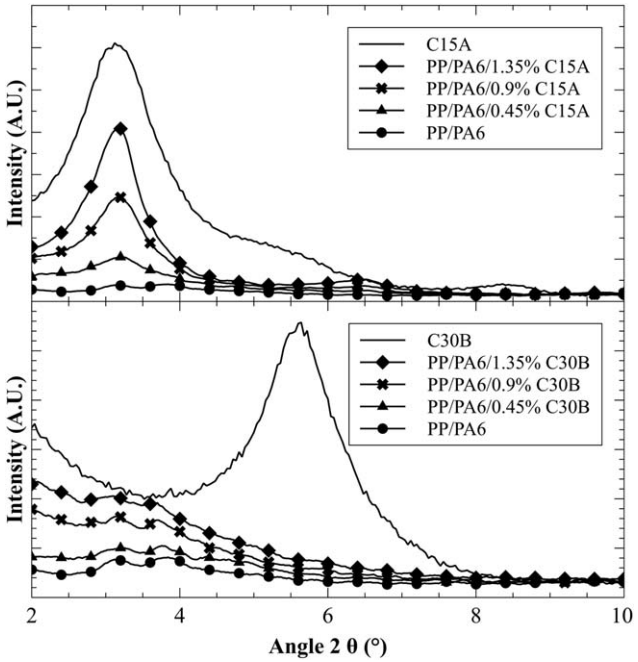

Figure 12. XRD patterns of PP/PA6/clay blends containing 0, 0.45, 0.9, and 1.35 wt % of C15A (top) or C30B (bottom).The corresponding clays are given as reference.

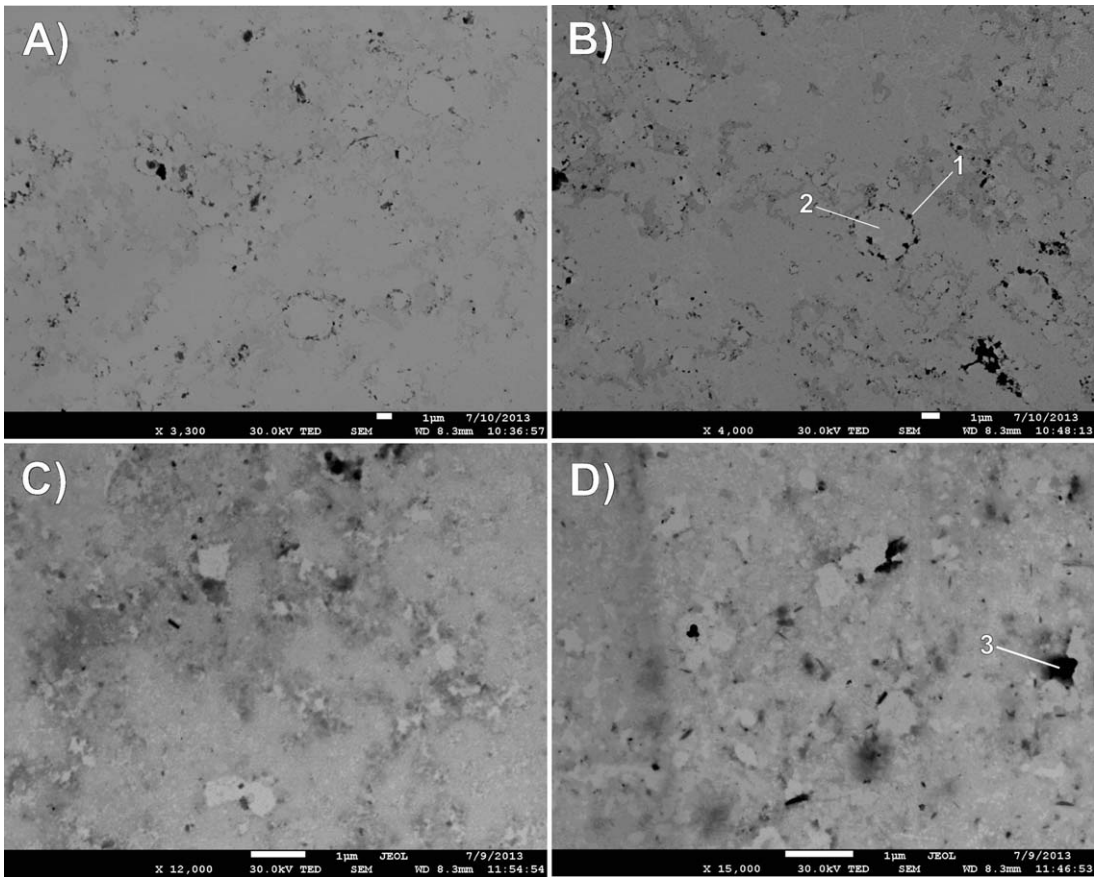

Figure 13. STEM micrographs of PP/PA6/0.9 wt % C15A (A, B) and PP/PA6/0.9 wt % C30B (C, D) blends (transverse view). The scale bar denotes 1 μm.

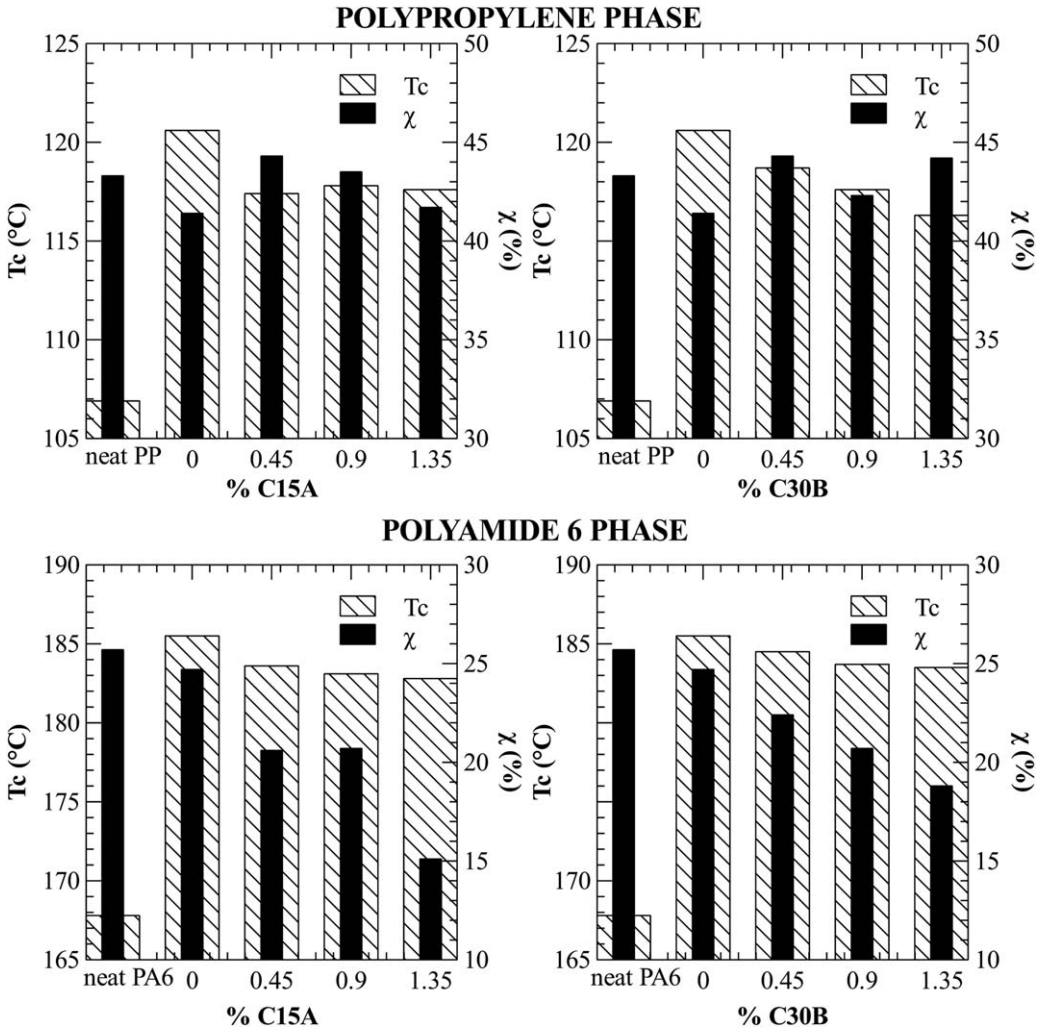

Figure 14. Crystallization temperature (T_c) and degree of crystallinity (χ) of PP, PA6 and PP/PA6 blends with 0, 0.45, 0.9, and 1.35 wt % of C15A or C30B.

assume to consider the nanofiller at its initial localization for the calculation (C15A in PP, C30B in PA6). The validity of this hypothesis has some limits as particle migration occurs during process, but it enables to obtain a general trend explaining the morphology evolutions. As the mixing process develops shear rates in the order of magnitude of 100 s^{-1}, it is more relevant to compare viscosity ratios at high frequency. In these conditions, it appears that C15A addition induces a decrease in viscosity ratio from 3 (0% C15A) to 2 (1.35% C15A) which is known to facilitate the dispersion of polymers in shear flow. A different trend is observed upon C30B addition: the viscosity ratio rises significantly above the recommended values ($k > 4$), justifying the difficulties of dispersion observed.

The elasticity has also been investigated through the ratio G'(PA6)/G'(PP) (Figure 11). For the unfilled blend, the graph shows that the elasticity ratio k' fluctuates between 0.5 and 2. The addition of C15A leads to the decrease of k', i.e. the matrix elasticity becomes larger relatively to the minor phase elasticity. This configuration is known to promote the dispersion efficiency.[4,26] With the C30B, k' reaches values far above unity, thus considerably restricting the possibilities to deform PA6 domains. Hence, the viscosity and elasticity data provide the explanation of the different morphologies obtained, depending on the mixing process and on the type of modified clay.

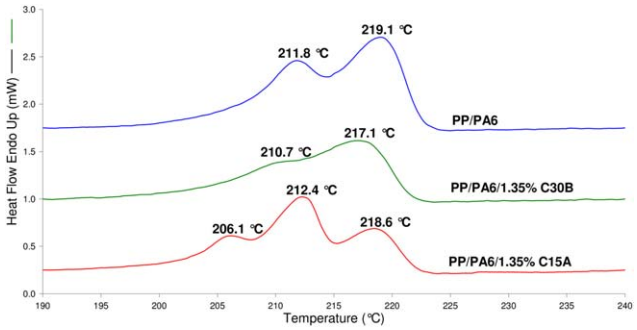

Figure 15. Melting endotherms (2nd heating) of PA6 in PP/PA6, PP/PA6/1.35 wt % C30B and PP/PA6/1.35 wt % C15A blends. [Color figure can be viewed in the online issue, which is available at wileyonlinelibrary.com.]

To check the evolution of nanoclay dispersion, X-ray diffraction experiments have been performed for each blend (Figure 12). For the PP/PA6/C15A blends, the diffraction peak is unchanged compared to the pure C15A. Hence, there is no visible extent of intercalation induced by the melt blending. A thermal degradation of the ammonium surfactant can be involved in that result.[27,28] On the contrary, for the PP/PA6/C30B blends, one can observe the absence of a clear diffraction peak, which is consistent with an exfoliated structure. Some small diffraction signals are visible between 3° and 4° but comparison with the unfilled blend show that it is independent of clay addition.

STEM analyses have been conducted to highlight nanoclay distribution in the different blends (Figure 13). It appears that C15A, initially dispersed in the polypropylene phase (the matrix), moved preferentially to the PP/PA6 interface (arrow 1), hence underlying the edges of the PA6 domains (arrow 2). A different trend is visible with the C30B. In that latter case, the localization of the filler remains unclear and only a few aggregates are visible on the micrographs (arrow 3). According to XRD and rheological data, we assume that most of the C30B is dispersed at a nanometric scale in the PA6 and thus cannot be seen in the range of magnifications available.

DSC measurements have been carried out for the different blends and for the neat polymers (Figure 14). The first observation is that blending neat PP and PA6 involves a strong increase in the crystallization temperatures of each component. For example, T_c of polypropylene rises from 107°C to ~120°C for the PP/PA6 blend. This result suggests a nucleating effect of already crystallized PA6 on melted PP, during the cooling process.[29] For the PA6, the increase of the crystallization temperature is generally explained in terms of process-induced molecular reorganization, due to hydrogen bondings.[30] A decrease in PP crystallization temperature occurs when adding C15A or C30B to the PP/PA6 blend. The hypothesis is that clay particles are partly located at the PP/PA6 interface and develop a barrier effect, thus inhibiting the nucleation from PA6. The fact that PP degree of crystallinity is not affected by the nanofiller and fluctuates around an average value of 42% tends to confirm that hypothesis. For the PA6, the crystallization temperature undergoes the same limited decrease with clay content but, in that case, the degree of crystallinity is also decreasing, from 21% down to 12%. These results suggest that in both cases clay platelets seem to be located in the PA6 phase or at the interface. The decrease of PA6 crystallinity could be due to the nanofiller that hinders the reorganization of PA6 macromolecules, limiting the possibilities of crystallization. The melting profile of PA6 crystallites is interesting as well (Figure 15). Actually, it appears that crystallites melt at lower temperatures when nanoclay is added. In particular, C15A addition leads to the apparition of specific crystallites with low melting point (206°C), indicating possible melting/re-crystallization phenomena. This demonstrates the creation of imperfect crystals due to the presence of nanofillers in the PA6. In conclusion, STEM micrographs combined with DSC analyses allow to conclude on the localization of C15A and C30B montmorillonites in the PA6 phase or at the PP/PA6 interface whatever the blending process, due to high PA6-clay polar affinity. Therefore, it means that a

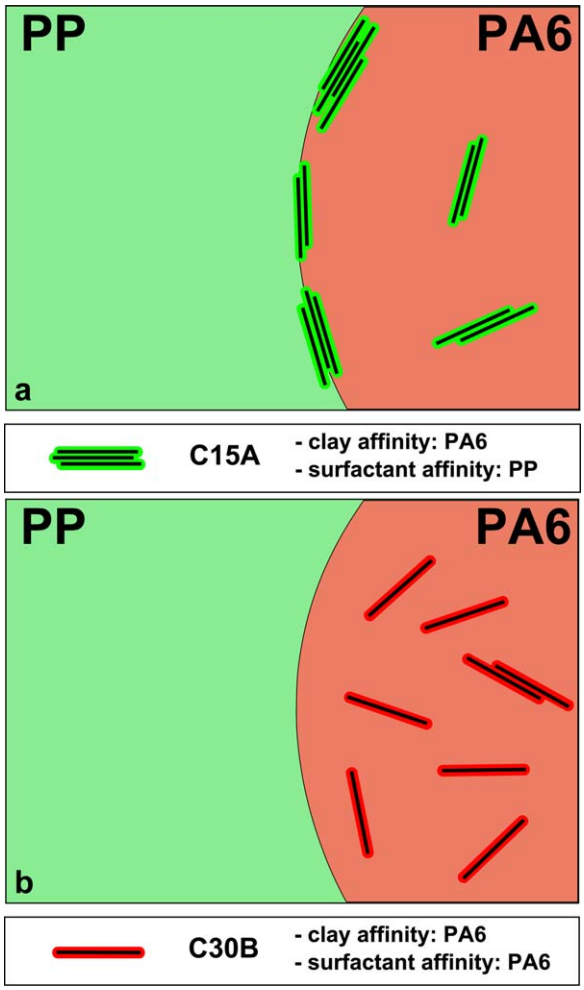

Figure 16. Schematic representation of the distribution and dispersion of C15A (a) and C30B (b) in PP/PA6 blends, linked to clays and surfactants affinities. [Color figure can be viewed in the online issue, which is available at wileyonlinelibrary.com.]

filler migration from PP to PA6 occurred during the processing of PP/PA6/C15A blends. In that latter case, the specific presence of numerous platelets at the interface results from the surfactant chemical structure. Indeed, C15A surfactant having better affinity with polypropylene than polyamide, it is more inclined to interact with the PP phase, thus blocking some platelets at the interface (Figure 16). Therefore, opposite forces control the migration of C15A: clay affinity with PA6 is partly counterbalanced by surfactant affinity for PP. The interfacial agent configuration of C15A justifies as well the reduction of domain sizes shown previously.

It has been shown that the presence of clay influences significantly the morphology, through the modification of viscosity and elasticity ratios. It is thus of prime importance to see how the microstructural evolutions impact the flow behavior. Therefore, some rheological measurements have been conducted on the different blends. In absence of organoclay, PP/PA6 storage modulus follows the same pattern than neat polypropylene at high frequency and then deviates at lower frequencies (Figure 17). This behavior is characteristic of the relaxation of the PA6

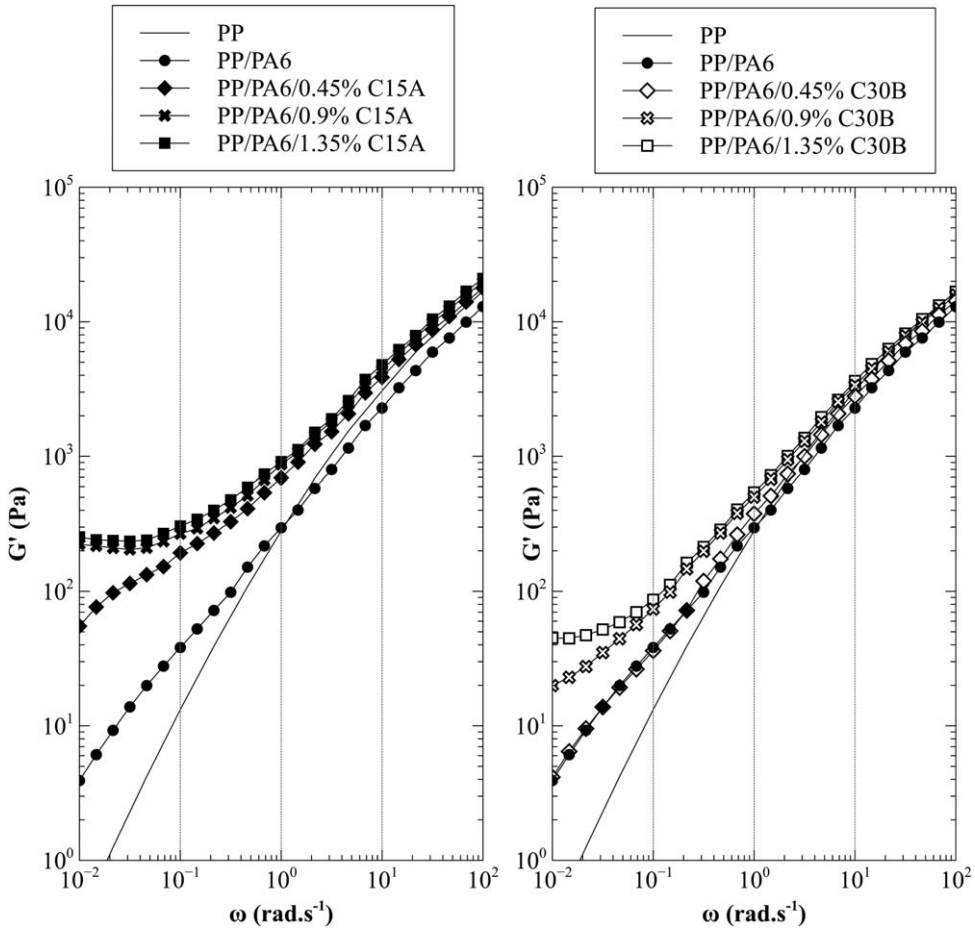

Figure 17. Storage modulus (G') of PP/PA6/C15A blends (left) and PP/PA6/C30B blends (right) with 0, 0.45, 0.9, and 1.35 wt % of clay. The PP storage modulus is given as reference.

minor phase and is closely linked to the interfacial tension. For the PP/PA6/clay blends, this phenomenon is more pronounced, leading to a non-terminal behavior at high clay content, for both types of clay. That low-frequency storage modulus plateau is usually ascribed to clay percolated networks restraining the relaxation processes through physical entanglements in the case of nanocomposites. It is worth noting that C15A leads to a higher and wider modulus plateau than C30B for a same montmorillonite content, contrary to what was observed for nanocomposites. Hence, it gives some evidence of a more developed network with the C15A.

Considering the complex viscosity η^* (Figure 18), it appears that PP/PA6 viscosity is quite similar to the one of neat polypropylene. Apparently, the 15% of PA6 doesn't have much influence on the viscosity because of the weak phase adhesion. Upon clay addition, the blends experienced a strong viscosity increase at low frequency, either with C15A or C30B. In particular, η^* tends to infinity for blends containing 1.35% of montmorillonite, which is typical of a solid-like behavior.

To evaluate the influence of clay nanoplatelets dispersed in the blends, these rheological data have been fitted with a modified Carreau–Yasuda law in a similar way as nanocomposites previously. The apparent yield stress values show that physical interactions are much more developed in PP/PA6/C15A blends than in PP/PA6/C30B blends (Table III). Such a difference in yield stresses cannot rely exclusively on the level of clay dispersion. Actually, XRD data have demonstrated that the dispersion of C30B is better than that of C15A in PP/PA6 blends, indicating that the answer is not to be found at the nanometric scale. Thus, the microstructure can be the key: SEM micrographs have shown a finely dispersed fibrillar morphology with C15A whether C30B lead to a coarse nodular morphology. In the latter case, the hypothesis is that each PA6 nodule contains a percolated network of well dispersed clay platelets but, due to the microstructure, these networks are isolated from each over. For the C15A case, a double percolation mechanism may be possible, i.e. each PA6 fibril contains a percolated network of clay platelets/tactoids and, thanks to the fibrils large aspect ratio, some fibrils are connected with their neighbors, thus extending the clay network range to the entire material (Figure 19).

Microstructural observations as well as rheological data gave some evidence about a potential lessening in interfacial tension upon clay addition. To further investigate this question, the weighted relaxation spectra of the different blends have been calculated from the rheological data. Actually, it is possible to

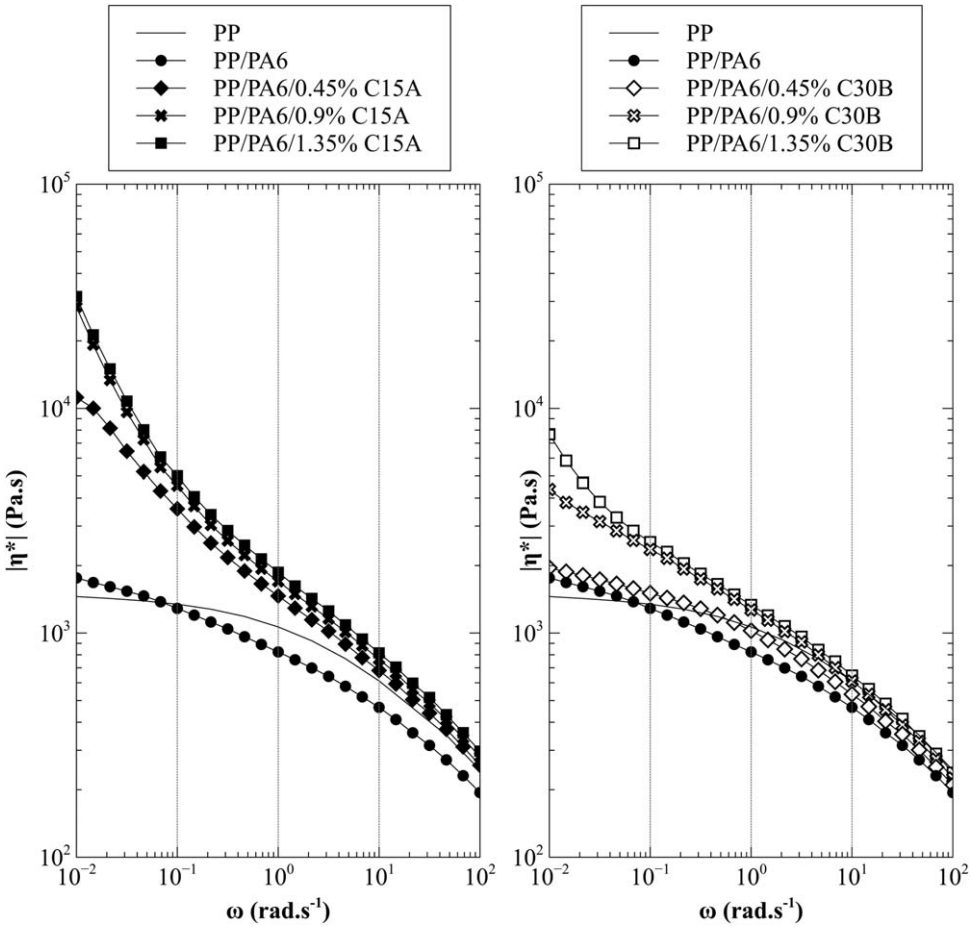

Figure 18. Complex viscosity ($|\eta^*|$) of PP/PA6/C15A blends (left) and PP/PA6/C30B blends (right) with 0, 0.45, 0.9, and 1.35 wt % of clay. The PP viscosity is given as reference.

infer the interfacial tension σ from these spectra,[31] using the following equation.[32]

$$\sigma = \frac{\eta_m R(19k+16)(2k+3)}{40\lambda(k+1)} \Big/ \left[1+\varphi\frac{5(19k+16)}{4(k+1)(2k+3)}\right] \quad (5)$$

where η_m is the matrix Newtonian viscosity (Pa s^{-1}), R is the radius of the inclusions (m), k is the viscosity ratio, ϕ is the volumic fraction and λ is the interface relaxation time (s). Figure 20 displays the relaxation spectra of polypropylene, polyamide 6, PP/PA6 and of a representative example of PP/PA6/montmorillonite blend (PP/PA6/0.9%C30B). For the PP/PA6 blend, three peaks can be isolated, corresponding to three major relaxation times. One can be ascribed to the matrix relaxation (0.11 s), one to the minor phase relaxation (27.7 s) and, by inference, the last one is characteristic of the interface (1.47 s). Using eq. (5), an interfacial tension of 5 mN m^{-1} can be calculated, which is in agreement with values found in the literature.[33] Hence, this method seems to be valid for the unfilled blend. For the example blend containing organoclay, only a single broad signal with a shoulder can be identified. In fact, clay platelets seem to impose a specific relaxation pattern overwhelming the other relaxation peaks and reaching its maximum outside the available frequency range. This method proved thus to be inappropriate for blends containing networks of dispersed nanofillers and should be restricted to truly binary blends.

Table III. Apparent Yield Stress (σ_0) in PP/PA6/C15A and PP/PA6/C30B Blends

Nanocomposites	σ_0 (Pa)	Nanocomposites	σ_0 (Pa)
PP/PA6/0.45% C15A	74	PP/PA6/0.45% C30B	1
PP/PA6/0.9% C15A	246	PP/PA6/0.9% C30B	10
PP/PA6/1.35% C15A	275	PP/PA6/1.35% C30B	48

Values obtained by modified Carreau–Yasuda law regression

CONCLUSIONS

In situ fibrillation of polypropylene/polyamide 6 blends containing two types of Cloisite® organoclay—differing by the polarity of their surfactants (low-polarity for C15A and high-polarity for C30B)—was investigated. Depending on the mixing process and on the type of organoclay, fibrillar- or nodular-like morphologies were obtained. The dispersion of C15A in the PP matrix was found to be the most suitable configuration to achieve a microfibrillar polymer/polymer composite structure with improved compatibility. Actually, in that case, a migration of the nanofiller occurred from the PP to the PA6 phase, leading to the accumulation of platelets at the interface. These platelets

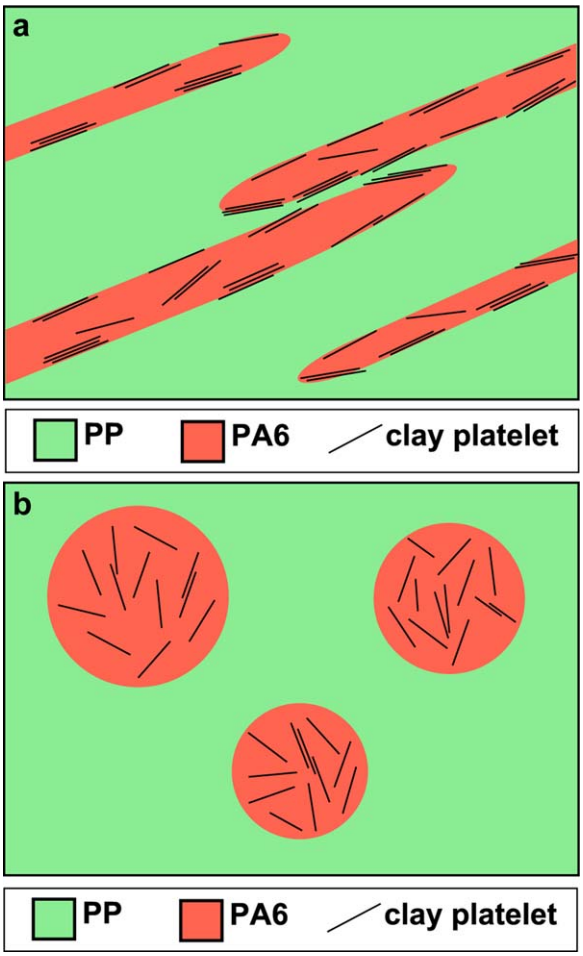

Figure 19. Schematic representation of the clay percolation range for fibrillar PP/PA6/C15A blends (a) and for nodular PP/PA6/C30B blends (b). [Color figure can be viewed in the online issue, which is available at wileyonlinelibrary.com.]

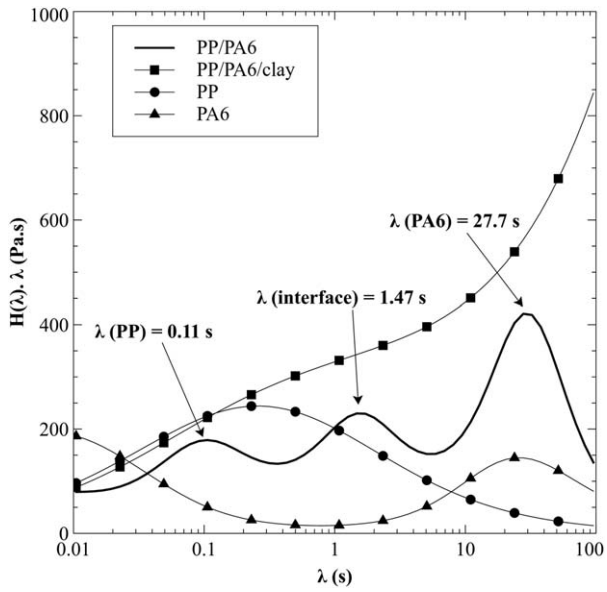

Figure 20. Weighted relaxation spectrum ($H(\lambda).\lambda$) of PP, PA6, PP/PA6, and PP/PA6/0.9 wt % C30B blends.

played a role of interfacial agent, restraining the coalescence and relaxation mechanisms. Conversely, the dispersion of C30B in the minor phase induced a degradation of the microstructure. In that latter case, the organoclay was unable to reach the interface and moreover a drastic increase in viscosity and elasticity ratios was evidenced, limiting the efficiency of shear mixing. Based on rheological results, a nanoclay double-percolation hypothesis is made for PP/PA6/C15A microfibrillar composites. Measurements of interfacial tension between PP and PA6 have been attempted using a rheological approach. However, this method proved to be ineffective with clay filled blends and needs further investigations. It is thus not possible to be affirmative concerning a reduction of interfacial tension. Finally, this study evidenced a possible use of nanoclays as "rheological modifiers," giving the possibility to adjust the viscoelastic properties of one phase in a polymer blend, so as to obtain advantageous viscosity and elasticity ratios, especially for *in situ* fibrillation purposes.

ACKNOWLEDGMENTS

The authors gratefully acknowledge the International Campus on Safety and Intermodality in Transportation (CISIT), the Nord-Pas-de-Calais Region and the European Community (FEDER funds) for their financial support.

REFERENCES

1. Shields, R. J.; Bhattacharyya, D.; Fakirov, S. *J. Mater. Sci.* **2008**, *43*, 6758.
2. Utracki, L. A.; Shi, H. *Polym. Eng. Sci.* **1992**, *32*, 1824.
3. Ghodgaonkar, P. G.; Sundararaj, U. *Polym. Eng. Sci.* **1996**, *36*, 1656.
4. Mighri, F.; Carreau, P. J. *J. Rheol.* **1998**, *42*, 1477.
5. Friedrich, K.; Evstatiev, M.; Fakirov, S.; Evstatiev, O.; Ishii, M.; Harass, M. *Compos. Sci. Technol.* **2005**, *65*, 107.
6. Fakirov, S.; Bhattacharyya, D.; Lin, R. J. T.; Fuchs, C.; Friedrich, K. *J. Macromol. Sci. B Phys.* **2007**, *46*, 183.
7. Tucker, C. L., III; Moldenaers, P. *Annu. Rev. Fluid Mech.* **2002**, *34*, 177.
8. Denchev, Z. Z.; Dencheva, N. V. *Polym. Int.* **2008**, *57*, 11.
9. Sinha Ray, S.; Pouliot, S.; Bousmina, M.; Utracki, L. A. *Polymer* **2004**, *45*, 8403.
10. Khatua, B. B.; Lee, D. J.; Kim, H. Y.; Kim, J. K. *Macromolecules* **2004**, *37*, 2454.
11. Sinha Ray, S.; Bousmina, M. *Macromol. Rapid Commun.* **2005**, *26*, 450.
12. Sinha Ray, S.; Bousmina, M. *Macromol. Rapid Commun.* **2005**, *26*, 1639.
13. Si, M.; Araki, T.; Ade, H.; Kilcoyne, A. L. D.; Fisher, R.; Sokolov, J. C.; Rafailovich, M. H. *Macromolecules* **2006**, *39*, 4793.
14. Dharaiya, D. P.; Jana, S. C. *J. Polym. Sci. B Polym. Phys.* **2005**, *43*, 3638.
15. Hong, J. S.; Namkung, H.; Ahn, K. H.; Lee, S. J.; Kim, C. *Polymer* **2006**, *47*, 3967.

16. Hong, J. S.; Kim, Y. K.; Ahn, K. H.; Lee, S. J.; Kim, C. *Rheol. Acta* **2007**, *46*, 469.
17. Honerkamp, J.; Weese, J. *Rheol. Acta* **1993**, *32*, 65.
18. Brandrup, J.; Immmergut, E. In Polymer Handbook, 3rd ed.; Wiley-Interscience Publication: New York; Chichester; Brisbane; Toronto; Singapore, **1989**.
19. Wagener, R.; Reisinger, T. J. G. *Polymer* **2003**, *44*, 7513.
20. Vermant, J.; Ceccia, S.; Dolgovskij, M. K.; Maffettone, P. L.; Macosko, C. W. *J. Rheol.* **2007**, *51*, 429.
21. Vergnes, B. *Int. Polym. Process.* **2011**, *26*, 229.
22. Soulestin, J.; Rashmi, B. J.; Bourbigot, S.; Lacrampe, M.-F.; Krawczak, P. *Macromol. Mater. Eng.* **2011**, *297*, 444.
23. Alix, S.; Follain, N.; Tenn, N.; Alexandre, B.; Bourbigot, S.; Soulestin, J.; Marais, S. *J. Phys. Chem. C* **2012**, *116*, 4937.
24. Sundararaj, U.; Macosko, C. W.; Rolando, R. J.; Chan, H. T. *Polym. Eng. Sci.* **1992**, *32*, 1814.
25. Potente, H.; Bastian, M.; Bergemann, K.; Senge, M.; Scheel, G.; Winkelmann, T. *Polym. Eng. Sci.* **2001**, *41*, 222.
26. Mighri, F.; Ajji, A.; Carreau, P. J. *J. Rheol.* **1997**, *41*, 1183.
27. Yousfi, M.; Soulestin, J.; Vergnes, B.; Lacrampe, M. F.; Krawczak, P. *J. Appl. Polym. Sci.* **2013**, *128*, 2766.
28. Yousfi, M.; Lepretre, S.; Soulestin, J.; Vergnes, B.; Lacrampe, M. F.; Krawczak, P. *J. Appl. Polym. Sci.* **2013**, *131*.
29. Marco, C.; Ellis, G.; Gómez, M. A.; Fatou, J. G.; Arribas, J. M.; Campoy, I.; Fontecha, A. *J. Appl. Polym. Sci.* **1997**, *65*, 2665.
30. Khanna, Y. P.; Reimschuessel, A. C.; Banerjie, A.; Altman, C. *Polym. Eng. Sci.* **1988**, *28*, 1600.
31. Demarquette, N. R.; De Souza, A. M. C.; Palmer, G.; Macaubas, P. H. P. *Polym. Eng. Sci.* **2003**, *43*, 670.
32. Gramespacher, H.; Meissner, J. *J. Rheol.* **1992**, *36*, 1127.
33. Palmer, G.; Demarquette, N. R. *Polymer* **2005**, *46*, 8169.